

# AGN FEEDBACK AND COOLING FLOWS: THE FAILURE OF SIMPLE HYDRODYNAMICAL MODELS

JOHN C. VERNALEO AND CHRISTOPHER S. REYNOLDS

Department of Astronomy, University of Maryland, College Park, MD 20742

*Draft version February 7, 2020*

## ABSTRACT

In recent years it has become increasingly clear that Active Galactic Nuclei, and radio-galaxies in particular, have an impact on large scale structure and galaxy formation. In principle, radio-galaxies are energetic enough to halt the cooling in the inner regions clusters, solving the cooling flow problem and explaining the high-mass truncation of the galaxy luminosity function. We explore this process through a series of high resolution, three dimensional hydrodynamic simulations of jetted active galaxies which act in response to cooling-mediated accretion of an ICM atmosphere. We find that such models are incapable of producing a long term balance of heating and cooling; catastrophic cooling can be delayed by the jet action but inevitably takes hold. At the heart of the failure of these models is the formation of a low density channel through which the jet can freely flow, carrying its energy out of the cooling core. While this obviously highlights the need to include physics beyond the ideal hydrodynamics considered here, it also underscores the importance of including jet dynamics in such models as opposed to the isotropically inflated bubble approach.

*Subject headings:* cooling flows — galaxies: active — galaxies: formation — galaxies: jets — hydrodynamics — X-rays: galaxies: clusters

## 1. INTRODUCTION

In recent years, it has become increasingly clear that Active Galactic Nuclei (AGN) may well have an impact on large scale structure and galaxy formation. The accepted framework for galaxy formation states that baryonic matter falls into developing dark matter halos, the resulting accretion shocks raising it to the approximately the virial temperature of the halo. The “cold” baryonic components of the galaxy then form via radiative cooling of this shocked gas. In the absence of any feedback processes (i.e., with gravitational collapse followed by radiative cooling alone), the galaxy mass function would have to essentially follow the dark matter halo mass function — in essence, the baryons that are within the turn-around radius of the developing dark matter halo are trapped and fated to eventually form the baryonic galaxy at the halo’s center. However, as has been long known, this is clearly not the case. At both the highest and lowest masses, there is a deficit of galaxies compared with dark matter halos. These major discrepancies indicate that multiple, non-gravitational, feedback mechanisms act on galaxy formation.

At the low luminosity/mass end of the galaxy distribution, the deficit can be explained entirely by feedback from star formation (Larson 1974; Dekel & Silk 1986). Once the (massive) first stars to form from the cooling baryons start to supernova, superwinds from the proto-galaxy can expel a significant fraction of the remaining baryons from the (shallow) gravitational potential well of the dark matter halo. The explanation for the deficit at the high mass end is not so clear, though. Inefficient cooling (Rees & Ostriker 1977) of baryons that have been shocked to the high virial temperature (exceeding  $10^7$  K) of large dark matter halos can account for some of the deficiency but is insufficient. An additional mechanism is required that is substantially more efficient than star

formation (e.g., see discussion in Benson et al. 2003). Many authors have suggested that radio-loud AGN provide this additional feedback.

If radio-loud AGN do indeed regulate the formation of the most massive galaxies, this is probably one of the few aspects of galaxy formation that can be studied in detail in the local universe: i.e., the cores of cooling galaxy clusters. Galaxy clusters possess the largest dark matter halos found in the Universe and contain virial baryons (the intracluster medium, or ICM) at X-ray emitting temperatures. The ICM of galaxy clusters has been intensively studied by every X-ray observatory since its discovery in the earliest days of X-ray astronomy (Felten et al. 1966), but imaging spectroscopy by *Chandra* and *XMM-Newton* have raised these studies to an unprecedented level. At its simplest, these observations provide measurements of the density and temperature of the ICM, which allows a radiative cooling time to be computed. In the central regions of most relaxed clusters, the cooling time is often significantly shorter than a Hubble time (and often as low as  $10^8$  years). With such short cooling times, there must be either a growing “sink” of cooled gas or a heat source acting on the cluster center. Observationally, there are very strong limits of the amount of cool gas present. In particular, there is no strong star formation seen in the central cD galaxy (although there is clearly star formation occurring at a low level (O’Dea et al. 2004)). The detailed discrepancy between the X-ray measured cooling rate and the lack of cooled gas forms the classic “cooling flow problem” (Fabian 1994). Dispersive spectroscopy by *XMM-Newton* deepened this mystery. While most clusters clearly show evidence for radiative cooling of the ICM from the virial temperature  $T_{\text{vir}}$  to about  $T_{\text{vir}}/3$ , the absence of lower-ionization iron lines sets tight limits on the emission measure of gas below  $T_{\text{vir}}/3$  (which would be expected to be a prolific radiator!).

Of course, there is an obvious link between the apparent inability of the ICM to cool below X-ray emitting

temperatures and the deficit of massive galaxies. It is precisely the cD galaxies at the center of rich galaxy clusters which are “trying” to grow above the observed cutoff in the galaxy mass function via the radiative cooling of the core regions of the ICM. This connection strongly suggests that solutions to the cooling flow problem that rely on “hiding” the signatures of cooling (e.g., through strong metallicity inhomogeneities or mixing layers) are doomed to fail, thereby increasing the motivation for providing a viable heat source for the cluster core.

Radio-loud AGN are very energetic and are frequently found in the giant elliptical (cD) galaxies in the center of cooling clusters (Burns & Owen 1977), which makes them ideal candidates for the heat source needed to offset cooling cluster. Even putting galaxy formation and cooling flow arguments aside, however, it is clear that radio loud AGN have an impact on their environment. First seen in *Einstein* and *ROSAT* observations (Feigelson et al. 1987; Böhringer et al. 1993, 1995; Carilli et al. 1994; Heinz et al. 1998), *Chandra* has studied numerous examples of ICM bubbles (Fabian et al. 2000; McNamara et al. 2000; Blanton et al. 2001; Young et al. 2002), ghost bubbles (McNamara et al. 2001; Heinz et al. 2002; Choi et al. 2004; Fabian et al. 2000), ripples (Fabian et al. 2003, 2005b), shells (Fabian et al. 2000), and filaments that are clearly associated with a central radio-loud AGN. There is a large body of numerical work which models various aspects of these interactions. Early hydrodynamic models of the putative jet-cocoon/shock structure in Cygnus-A were presented by (Clarke et al. 1997). More recent numerical investigations have explored the buoyant evolution of the cocoon after its supersonic expansion phase (Churazov et al. 2001; Brüggén & Kaiser 2001, 2002; Reynolds et al. 2002; Robinson et al. 2004; Basson & Alexander 2003), the effect of plasma transport processes (Ruszkowski et al. 2004; Reynolds et al. 2005) and the action of magnetic fields (Robinson et al. 2004; Jones & De Young 2005).

Despite the reasons to look to AGN heating as the solution to the cooling flow problem (and hence the regulator of high mass galaxy formation), there is a problem with this picture. Direct observational signatures of ICM heating remain elusive in the observations despite the existence of some very deep *Chandra* and *XMM-Newton* observations of nearby vigorous ICM/AGN interactions. Strong shocks are not seen in most systems even though they are always seen in simulations with strong AGN heating. Furthermore, the recent sample of radio-galaxy blown ICM bubbles by Birzan et al. (2004) suggests that the total work done by the AGN on the ICM may not be sufficient (by approximately an order of magnitude) to offset cooling.

In this paper we perform high-resolution, three dimensional ideal hydrodynamic simulations of AGN feedback in a relaxed cooling cluster. Unlike many of the previous 3-d investigations (with the notable exception of Basson & Alexander (2003)), we simulate the injection of a supersonic jet into the ICM atmosphere rather than starting with an initial condition of a pre-inflated, static radio cocoon. We consider this an important issue — only through a direct modeling of the jet can we

hope to be able to capture the jet-induced ICM shock heating as well as the complex internal dynamics of the cocoon. While the effect of the jet on the ICM is treated from first principles (through the evolution of the equations of hydrodynamics), the enormous range of scales between the ICM core and the gravitational sphere of influence of the black hole prevents us from treating the AGN fueling properly. In this paper, we introduce several different feedback prescriptions by which the AGN jet power is related to the ICM properties in the innermost region. Our goal is to construct a model system in which AGN heating and ICM cooling are, in the long term, in balance. We find that all ideal hydrodynamic models *fail* to achieve this balance and, hence, argue that physics beyond that of ideal hydrodynamics must be crucial to the AGN feedback picture if, indeed, the picture is correct at all.

In Section 2, the basic setup for our simulations is described, including a description of the model ICM atmosphere and our hydrodynamic code. Section 3 presents our results for the different feedback scenarios considered. We discuss the results along with possible ways to redeem hydrodynamic jet models in Section 4. Finally our modifications to the ZEUS-MP code are explained in Appendix A.

## 2. BASIC SETUP

We aim to model the ICM of a cluster and its interaction with a central radio galaxy. Our basic picture is a spherical cluster consisting initially of stationary dark matter and gas. The gas is initially in hydrostatic equilibrium, but is cooling through optically thin thermal emission. As the gas cools, some of it will flow across the inner radial boundary of the simulation and is no longer simulated. The amount of gas to cross this boundary is used as our primary diagnostic of the cooling flow.

Initially, the cluster is spherically symmetric and isothermal. The gas is setup with a  $\beta$ -model profile,

$$\rho(r) = \frac{1}{[1 + (\frac{r}{r_0})^2]^{3/4}}. \quad (1)$$

This is a simple analytic fit to cluster mass profiles. The gravitational potential,

$$\Phi = \frac{c_s^2}{\gamma} \ln(\rho), \quad (2)$$

is the set so the initial gas configuration is in hydrostatic equilibrium. The potential is assumed to be generated by a static distribution of dark matter which remains fixed throughout the simulation. The self gravity of the gas is ignored (we note that in a standard cosmology, the gas mass is only around 14% of the total cluster mass (Ostriker et al. 2005)).

Spherical polar  $(r, \theta, \phi)$  coordinates are used. All simulations were run on a  $200 \times 200 \times 100$  cell grid, with enhanced resolution near the center of the cluster and near the jet axis. This corresponds to a physical grid with an inner radius at  $r = 10$  kpc and an outer radius at  $r = 1000$  kpc. The angular coordinate was only allowed to vary from  $\theta = 0$  to  $\theta = \frac{\pi}{2}$ . This effectively only covers half the cluster and therefore only allows for one jet. Reflecting boundaries were used to mimic the effect of the missing half of the cluster. This aids in maintaining

a high-resolution while keeping a reasonable number of grid cells.

In ideal (adiabatic) hydrodynamics, the equations of hydrodynamics can be written in dimensionless form and, hence, the results of a single simulation may be scaled to a whole family of problems with different mass, size and time scales (e.g., see Reynolds et al. (2002)). Since we must add radiative cooling to our simulations (see Section 3.1), we are forced into a set of physical units. The values for the rich cluster of Reynolds et al. (2002) were used. This gives us a core radius of  $r_o = 100$  kpc, a code length unit of  $r = 50$  kpc, time units of 50 Myrs, a sound speed  $c_s = 1000$  km s<sup>-1</sup>. The resulting radiative luminosity of the model ICM is  $1.22 \times 10^{45}$  erg s<sup>-1</sup>.

### 2.1. Code

The simulations were performed using the ZEUS-MP code. A modified version of the original National Center for Supercomputing Applications (NCSA) release was used. We have made our modified version publicly available<sup>1</sup>. A further discussion of this version of ZEUS-MP detailing our modifications is given in Appendix A.

ZEUS-MP is a parallel version of the ZEUS magneto-hydrodynamic code (Stone & Norman 1992a,b). ZEUS is a fixed-grid, time-explicit Eulerian code which uses an artificial viscosity to handle shocks. When operated using van Leer advection, as in this work, it is formally of second order spatial accuracy. The work reported here used this code in a pure hydrodynamic mode. All simulations were done on the University of Maryland, Astronomy Department's GNU/Linux Beowulf cluster with run times of the order of one to two months for four processor simulations.

ZEUS solves the standard hydrodynamic equations, which, including radiative cooling (Section 3.1) are

$$\frac{D\rho}{Dt} + \rho \nabla \cdot \mathbf{v} = 0, \quad (3)$$

$$\rho \frac{D\mathbf{v}}{Dt} = -\nabla P - \rho \nabla \Phi, \quad (4)$$

$$\rho \frac{D}{Dt} \left( \frac{e}{\rho} \right) = -P \nabla \cdot \mathbf{v} - \Lambda, \quad (5)$$

where

$$\frac{D}{Dt} \equiv \frac{\partial}{\partial t} + \mathbf{v} \cdot \nabla. \quad (6)$$

Stability is determined by the usual Courant-Friedrichs-Lewy (CFL) condition. As the jet is typically very supersonic, its speed provides the limiting timestep during most of the simulations.

## 3. SPECIFIC MODELS

A set of thirteen 3-d simulations were performed. Table 1 lists the simulations along with some relevant parameters. In the following sections we will describe each simulation along with presenting the results of each.

An important diagnostic used to compare the different models was the mass accretion rate across the inner boundary of the simulated grid. This was measured in

TABLE 1  
LIST OF SIMULATIONS

Name	Feedback	Efficiency	Delay	Rotation
Run A	none	NA	NA	NA
Run B	strong jet	NA	NA	NA
Run C	weak jet	NA	NA	NA
Run D	simple feedback	0.0001	NA	NA
Run E	simple feedback	0.00001	NA	NA
Run F	delayed feedback	0.0001	short	NA
Run G	delayed feedback	0.00001	short	NA
Run H	delayed feedback	0.0001	long	NA
Run I	delayed feedback	0.00001	long	NA
Run J	delayed feedback	0.01	long	NA
Run K	delayed feedback	0.1	long	NA
Run L	delayed feedback	0.00001	long	solid body rotation
Run M	delayed feedback	0.00001	long	Fraction of grav. rotation

$M_\odot$  year<sup>-1</sup>. To calculate the mass flow, the amount of mass in each cell on the inner boundary with a negative (inward) velocity in the radial direction was summed. This is probably not completely accurate at the highest densities and mass accretion rates as the inflow boundaries are not perfectly efficient and sound wave may be reflected off the boundary. However, this should not change the results since these inaccuracies do not occur until the mass flow and density reach physically unrealistic values.

### 3.1. Radiative cooling

The driving force behind the cooling flow is the thermal bremsstrahlung and line radiation which removes thermal energy from the ICM core. This is modeled with the optically thin cooling law

$$\Lambda = [C_1(k_B T)^\alpha + C_2(k_B T)^\beta + C_3] 0.704 (\rho/m_p)^2 \times 10^{-22} \text{ ergs cm}^{-3} \text{ s}^{-1}, \quad (7)$$

which is the same law used by Ruszkowski & Begelman (2002) with the coefficients  $C_1 = 8.6 \times 10^{-3}$ ,  $C_2 = 5.8 \times 10^{-2}$ ,  $C_3 = 6.4 \times 10^{-2}$ ,  $\alpha = -1.7$ , and  $\beta = 0.5$  (Sutherland & Dopita 1993). This cooling term is proportional to  $\rho^2$  which produces the eventual catastrophic cooling as the center of the cluster becomes denser as it cools. Below a minimum temperature (0.1 keV), cooling was manually truncated. Even if we allowed material to cool below this limit, our spatial resolution would be insufficient to follow the resulting structures and additional physics not captured by eqn. 7 would become applicable.

The cooling represents an extra term in the energy equation (eqn. 5) and is implemented as an explicit source term. As with all physical processes, there is a maximum allowed time step for numerical stability associated with the cooling, but in our case it is always above the normal hydrodynamic CFL condition and need never be implemented.

Due to the density dependence of the radiative cooling, it is only relevant in the inner regions of the cluster. This is important for three reasons. First, as the core cools, the inner regions loses pressure support. This causes the inward flow of material, some part of which could fuel the accretion on the central compact object. Second,

<sup>1</sup> <http://www.astro.umd.edu/~vernaleo/zeusmp.html>

as the inner regions become denser due to the sagging, the cooling increases. This causes the eventual runaway cooling whose absence represents part of the cooling flow problem. Finally, since the outer region does not cool appreciably with a Hubble time or so, it represents a large reservoir of hot material which could potentially be exploited to balance cooling (although this does not seem possible in purely hydrodynamic models).

To establish a control, our first simulation (Run A) followed the pure radiative collapse of our model ICM atmosphere (i.e., a spherically symmetric homogeneous cooling flow). The evolution of this system was very simple. The cluster cools, primarily in the inner regions. As it cools, the inner regions become denser. As the gas becomes denser, it cools quicker, and the process runs away (until numerical issues with the very cool dense gas force us to terminate the simulation). The mass accretion rate for pure cooling can be seen in Figure 1. With no mechanism to stop or slow the cooling, the mass accretion shows a featureless, approximately exponential increase. This unbounded cooling and mass accretion is our first example of a catastrophic cooling.

To diagnose the time taken for the system to undergo a cooling catastrophe, we measure the time taken for each of our simulations to exceed a mass accretion rate of  $5000 M_{\odot} \text{yr}^{-1}$  (an arbitrary “large” mass accretion rate). For the pure cooling flow run (Run A), this threshold mass accretion rate is crossed at 244.1 Myrs. Material first fell below our imposed lower temperature limit at 248.9 Myrs. The radial dependence of temperature for Run A is shown in Figure 2. Initially the cluster is isothermal. The inner regions cool first, while the outer regions barely change in temperature. As catastrophic cooling occurs, the temperature gradient in the inner region becomes progressively steeper.

### 3.2. Single AGN Outburst Models

The onset of the cooling catastrophe in the homogeneous cooling flow is well known and unsurprising. Our hypothesis and the focus of this work is the idea that jet activity by a central AGN can heat the ICM core and prevent this catastrophic cooling. As an initial exploration of jet heating models, we follow the evolution and effects of a period of jet activity in which the jet has a fixed and constant power for a pre-defined duration. In Run B, the jet is active for 50 Myrs after which it is completely shut off and the resulting ICM allowed to evolve passively. These cases are essentially 3-dimensional generalizations of the axisymmetric simulations of (Reynolds et al. 2002) and share many characteristics with (but are higher resolution than) Basson & Alexander (2003). This can be viewed as a zeroth order approximation to AGN feedback.

In detail, the action of the AGN is modeled as a jet of low density material injected from the inner radial edge of the simulation grid using an inflow boundary condition. The jet has a density of 1/100 of the initial inner ICM density and (at the inner boundary) is in pressure equilibrium with the initial inner ICM. Therefore, the internal sound speed of the injected jet material is 10 times that in the initial ICM atmosphere. The jet has an opening angle of  $15^\circ$ . In the case of a single jet outburst of Run B, a Mach number of around 10.5 compared to the background material was used resulting in a total kinetic

luminosity of  $9.8 \times 10^{45} \text{ erg s}^{-1}$ . We also modeled a rather weaker jet with kinetic luminosity of  $8.9 \times 10^{45} \text{ erg s}^{-1}$  in Run C (which was otherwise identical to Run B).

Plots of entropy are shown at various times for Run B in Figure 3. As discussed in Reynolds et al. (2002), plots of entropy are a good tool for differentiating shocked jet material from background material. Initially, the jet carves a path through the ICM, and terminates in a shock. It can be seen that the jet channel is surrounded by a backflow of shocked (high entropy) jet material. This shocked material is over-pressurized compared to the background, and expands laterally into a cocoon structure. The cocoon is separated from the background by a contact discontinuity. Rayleigh-Taylor (RT) and Kelvin-Helmholtz (KH) instabilities work to shred this cocoon and mix in background material. After the jet has been turned off, the cocoon is left to evolve passively. Buoyancy forces cause it to rise, leaving the cluster core. Once the cocoon completely detaches itself from the core, it takes on the appearance of a rising bubble, which spreads out and fades somewhat into the cluster background (much like observed ghost bubbles) until it leaves the computational grid.

Figure 4 shows mass accretion for Run B and Run C. Although these differ slightly in the timing, they qualitatively show the same behavior. Initially, there is moderate mass flow (a few hundred  $M_{\odot} \text{yr}^{-1}$ ). Ironically, the jet-activity is actually responsible for this initial enhanced period of inflow; some matter in the innermost region of the ICM core becomes caught in the backflow that results from the onset of the jet activity and is swept across the inner boundary. After the initial spike, the mass accretion rate drops off to very low values while the jet is on and remains very low for over 100 Myrs after the jet stops due to the shock heating of the ICM core. The cooling flow then starts to re-establish and the mass flow begins to increase (eventually) catastrophically as it does in the pure cooling case. The time for catastrophic cooling has been delayed somewhat from the pure cooling case. For Run B,  $\dot{M}$  does not reach  $5000 M_{\odot} \text{yr}^{-1}$  until 306 Myrs (more than 60 Myrs later than the pure cooling model). Material falls below the minimum cooling temperature at 305 Myrs (i.e., at essentially the same time that the mass accretion rate crosses our “catastrophe” threshold). The weaker jet, Run C, reaches the catastrophic point at 285 Myrs, which is only slightly delayed from the pure cooling case. The temperature falls below our floor at 274 Myrs (also slightly later than the pure cooling case).

### 3.3. Feedback Models

The radio-loud AGN feedback hypothesis would argue that the central AGN acts such as to maintain a long term balance of jet heating and radiative cooling of the ICM. Furthermore, this must occur in systems with widely varying radiative luminosities. Clearly, this mechanism requires that the AGN power be somehow regulated by conditions within the ICM so that it does not underheat or overheat the ICM core. In this work, we explore a set of models in which the kinetic luminosity of the jets is connected to the mass accretion rate in the cooling flow. Unlike the other effects (cooling, jets, etc.), feedback is the only one that does not directly represent fundamental physics of the cluster gas. Instead, it tells

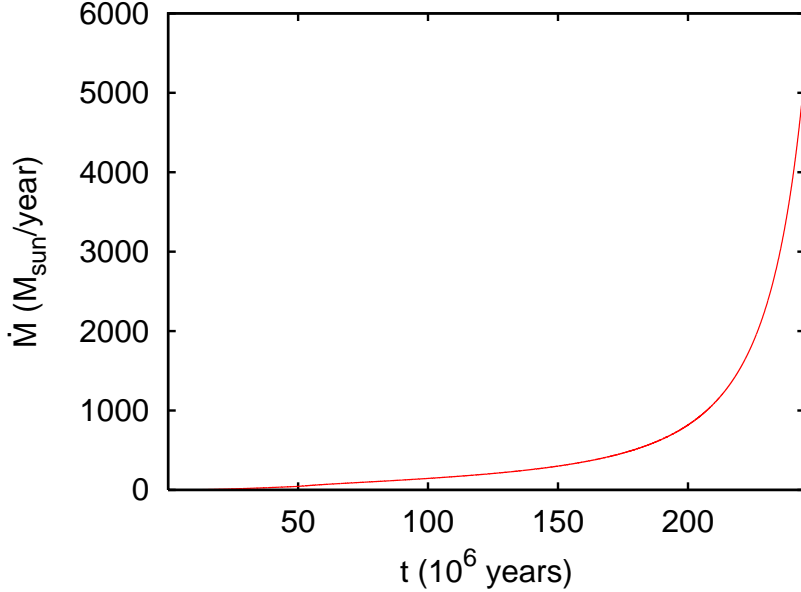


FIG. 1.— Mass accretion rate for pure cooling (Run A).

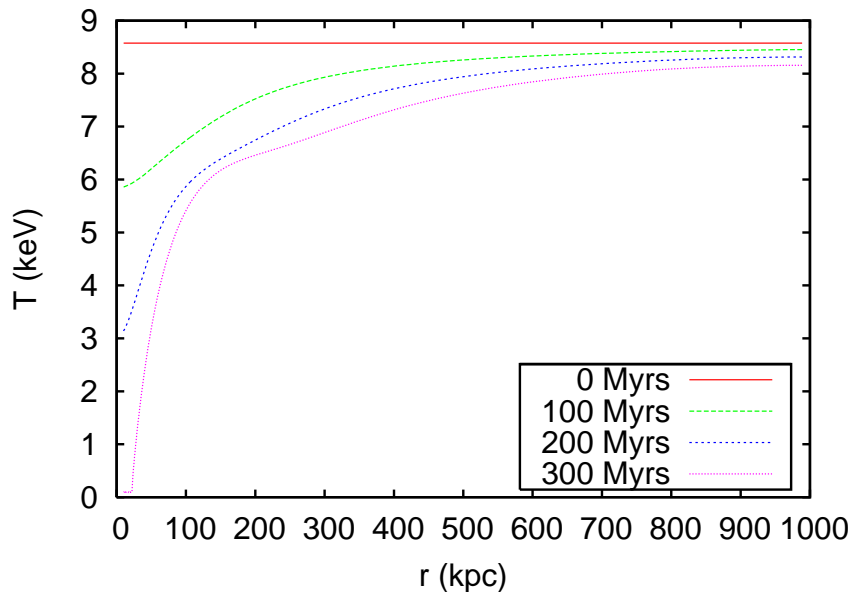


FIG. 2.— Radial temperature dependence for pure cooling (Run A).

us something about the central engine of the AGN. This provides us with the most freedom in how to implement it. Due to the large range of scales involved, it is not possible to directly model feedback. This would require resolving gas for the outer edges of the cluster (nearly a megaparsec) all the way down to the inner accretion disc (parsec scales). A direct assault on this problem would not be practical at the current time even for an Adaptive Mesh (AMR) code. Instead, we must use some simplified model for feedback.

In our first set of feedback simulations (Runs D and E), the jet is injected with a kinetic energy proportional to the instantaneous mass accretion rate across the inner radial boundary of our simulation domain. This is

achieved by modulating the injection velocity to be

$$v_{jet} = \left( \frac{2\eta \dot{M} c^2}{A\rho} \right)^{\frac{1}{3}}, \quad (8)$$

where  $\eta$  is the efficiency with which the rest mass energy of the ICM cooling flow is converted into jet power. The appropriate choice for  $\eta$  is far from clear. In the extreme case that *all* of the matter that flows across the inner boundary was to accrete onto the central supermassive black hole,  $\eta$  would be the jet-production efficiency of the actual black hole accretion disk itself. For an efficient disk, we would have  $\eta \sim 0.1$ , although higher efficiencies are possible if the black hole is spinning (Novikov & Thorne 1973) or if magnetic cou-

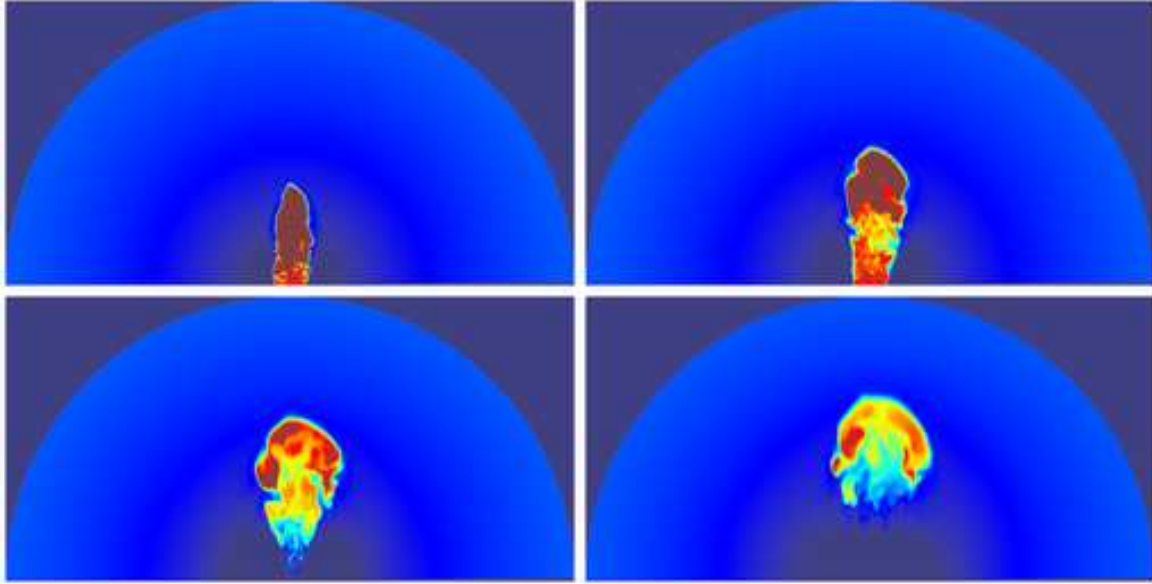


FIG. 3.— Entropy plots for single jet (Run B) at  $t=50, 125, 250,$  and  $375$  Myrs. The semi-circle in each plot represents the outer edge of the simulated grid at  $1000$  kpc.

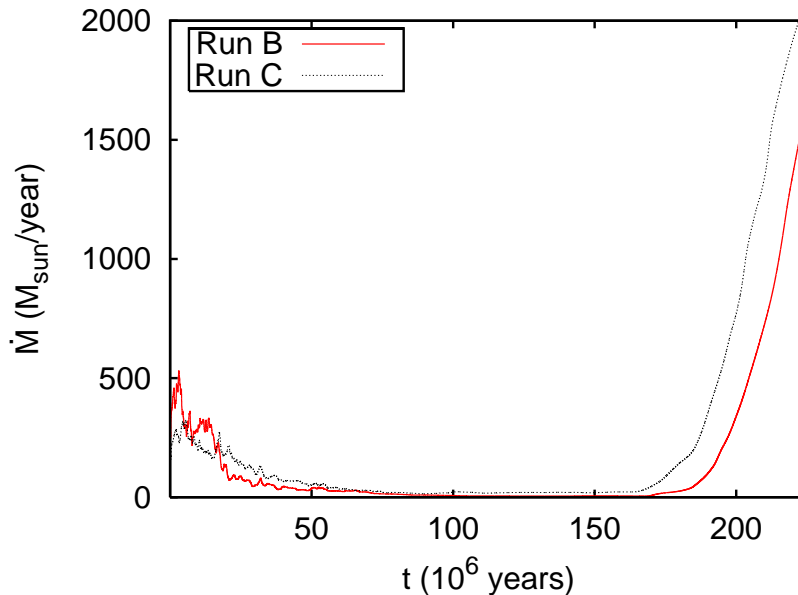


FIG. 4.— Mass accretion rate for single burst (Run B and Run C).

pling within the radius of marginal stability becomes important (Gammie 1999; Armitage & Reynolds 2003). However, as has been extensively discussed, supermassive black holes in the centers of giant elliptical galaxies accreting at a modest rate from the hot interstellar medium may well have a significantly smaller efficiency ( $\eta \sim 10^{-3}$ ). Much of the remaining energy is advected across the event horizon or driving a slow, uncollimated wind from the disk. Furthermore, it is plausible that only a small fraction of the mass that flows across the inner boundary of our simulation domain (located at  $10$  kpc) actually enters the sphere of influence of the massive black hole, with some of the remaining going to fuel low-level star formation.

Motivated by this discussion, we explored two cases of simple feedback with efficiencies of  $\eta = 10^{-4}$  (Run D) and  $\eta = 10^{-5}$  (Run E). The resulting mass accretion for Run E (lower efficiency) is given in figure 5. The higher efficiency (Run D) shows the same pattern. Initially, the mass accretion rate cycles up and down in response to the jet power (partly due to the backflow noted above), as we would expect if feedback works to stop cooling. However, by  $150$  Myrs, this breaks down. From that point on, the mass accretion rate increases, and the increasingly powerful jet does nothing to stop it. The time for catastrophic cooling and for material to fall below the minimum cooling temperature is not significantly affected by this type of feedback. Both runs have very sim-

ilar catastrophic cooling times with 246.7 Myrs for Run D and 245.43 for Run E. This is essentially the same as the time for the pure cooling model.

The reason for this failure of feedback to prevent the cooling catastrophe can be seen in Figure 6. After the jet has been active for a while (even at very low power) it clears a low-density channel in the ICM. As cooling and ICM accretion proceeds along equatorial latitudes (i.e., in the plane perpendicular to the jet axis), the increasingly powerful jet flows freely down the pre-cleared channel. This prevents the jet from depositing energy near the cluster core. Instead the kinetic energy is carried to the head of the cocoon reasonably unimpeded. With no energy deposition near the core, cooling proceeds on the catastrophic course in the equatorial regions almost as if there were no jet.

### 3.4. Delayed Feedback Models

The failure of the simple feedback model is, at least in part, related to the formation of the low density channel along the jet axis. Feedback prescriptions which allow this channel to collapse between powerful outbursts could, in principal, alleviate this problem.

Motivated by this, and in an attempt to model more realistic feedback, we performed a set of simulations in which a time delay was introduced between the mass accretion rate and the response of the jet. Clearly the immediate feedback of Run D and E is not physically accurate. Some time delay must be added to account for the material travel time from the inner edge of the grid to the accretion disk and onto the black hole. We note that the time for the relativistic jet to reach from the black hole and to enter the computational domain is negligible.

In Runs F and G, a delay of 10 Myrs was introduced. This is the sound crossing time of the cluster center (the area from the inner edge to  $r = 0$ ) and represents the minimum physically reasonable delay. Runs H, I, J, and K all have a delay time of 100 Myrs. This is approximately the dynamical time for the central galaxy and is a reasonable “best-guess” at a physically plausible time delay. Interestingly, this is also the approximate cooling time observed by *Chandra* in the centralmost regions of cluster cooling cores. The efficiencies of these runs is listed in Table 1.

An example of the low efficiency delayed feedback with a short delay can be seen in Figure 7. There is not much difference between this and the immediate feedback. There is also no essential difference in the time to reach catastrophic cooling. The only minor effect we see here is that the lower efficiency run (G) has a slightly lower rate of increase for the accretion, probably due to less efficient channel formation.

For Runs H through K, the physically motivated delay of 100 Myrs was used. Runs H and I are essentially copies of Runs F and G with a longer delay between the mass flow and the jet. As Figure 8 shows, this has a more significant effect on the mass flow than the shorter delay had. For the first 100 Myrs, there was no jet, so the run proceeded as a pure cooling run. The onset of (weak) jet activity caused a sharp dip in the accretion, followed by a spike (up to  $600 M_{\odot} \text{year}^{-1}$ ) lasting for about 50 Myrs (or half of the dynamic time). However, after several smaller smaller spikes and dips, runaway

cooling proceeds in the equatorial plane. In these cases, the cooling catastrophe is delayed as compared with the pure cooling model, but only by 40 Myrs. The higher efficiency version (Run H) behaved similarly only it reached the cooling catastrophe slightly faster (once again due to increased channel formation).

Given the difficulties with the feedback models found above, we also ran two simulations with *very* efficient jet production; Run J and K possessed  $\eta = 0.01$  and 0.1 respectively. Run K was performed in the spirit of an *extreme case* and we note that it is not reasonable that accretion onto the central galaxy and then onto the central AGN are both perfect, with the only loss coming from relativity and the central black hole. Even at an efficiency of 0.01 it is hard to come up with a plausible scenario for such nearly perfect accretion.

Even the extreme runs are not able to completely stop cooling. For Run J, the temperature falls below  $T_{\min}$  at 245 Myrs. This is even sooner than in the pure cooling case. Run K does not have this until 267 Myrs which is between the times for the other delayed runs and the single jet runs. The extreme efficiency feedback does, however, significantly delay catastrophic cooling. Run J does not experience catastrophic cooling until 345 Myrs. The mass accretion behavior is shown in Figure 9. Although it has taken longer for the cooling to reach our catastrophic level, the final catastrophe is extremely sharp, with the mass accretion rate exponentiating on timescales of only 1 Myr or so. This is much more dramatic than any of the less efficient runs. Run K holds off catastrophic cooling for 50 Myrs beyond Run J (398 Myrs), but it too becomes catastrophic rapidly at that point.

### 3.5. Feedback with Rotation

The AGN feedback and jet heating models described above clearly fail to adequately heat the ICM core in a manner that stably offsets radiative cooling. Our final two simulations (Runs L and M) explore the effect of an ICM atmosphere that is not initially static. The ICM of real clusters is never, of course, a perfect hydrostatic atmosphere. Clusters have complex merger and formation histories that leave an imprint on the dynamics of the ICM (Burns & Owen 1977). In several clusters observed with *Chandra*, the ghost cavities are not symmetric about the cluster center (e.g., A4059, Heinz et al. (2002); Perseus-A, Fabian et al. (2003)), suggesting that they are buoyantly rising in an ICM atmosphere which itself has velocity structure. While a full exploration of this class of models is beyond the scope of this paper, our final two simulations model the case of a rotating ICM atmosphere. Due to the assumed reflection symmetry in the plane perpendicular to the jet axis, we are forced to consider only rotations with an axis coincident with the jet axis.

In Run L, a delayed feedback model similar to Run I is examined in which the initial ICM atmosphere is assumed to undergo solid body rotation. The rotation speed at the outer edge of the grid is set equal to the sound speed of the cluster. This leaves the rotation in the core at a very low value. The results from this were nearly indistinguishable (in cooling, not in detailed physical structure) from Run I. This is because the rotation in the core was not high enough to mix the ICM effectively or stop accretion in any other way. Without having gas

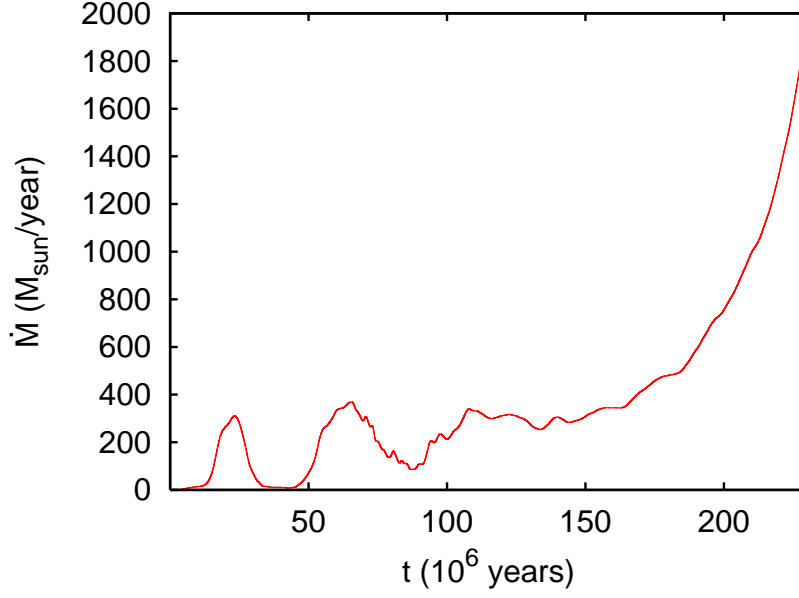


FIG. 5.— Mass accretion rate for feedback model (Run E).

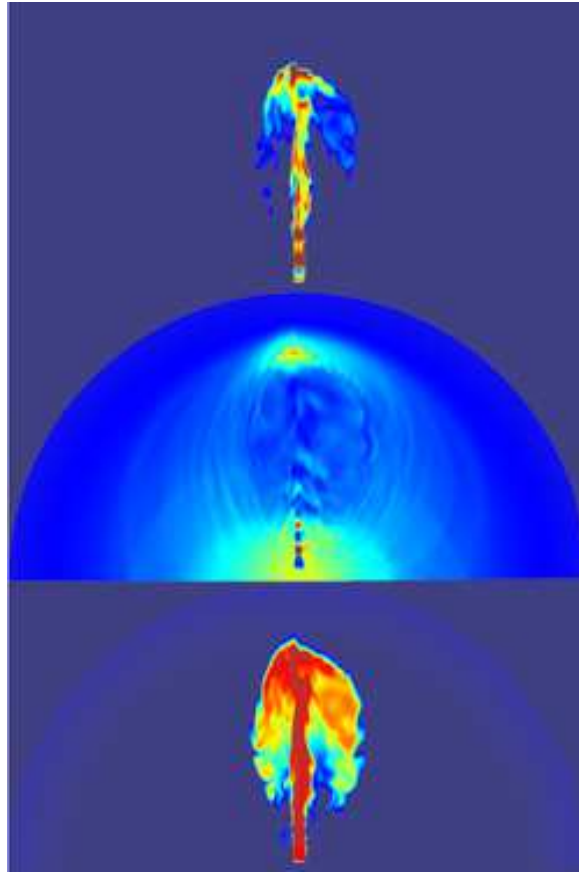


FIG. 6.— Temperature Map (top), Pressure Map (middle), Entropy Map (bottom) for immediate feedback jet. The temperature map only shows the highest temperatures to pick out primarily jet material. The thin, low density channel can be easily seen in temperature and pressure (and to a lesser extent entropy). Only the inner 254 kpc of the simulation is shown.

moving supersonically in the outer parts of the cluster (which is clearly unphysical), there is no way to get solid body rotation to help offset cooling.

In Run M a rotation law was chosen such that the

centrifugal force associated with the rotation is a fixed fraction (10%) of the gravitational force at that location. This results in a rotation law in which the angular velocity increases with decreasing radius until one gets



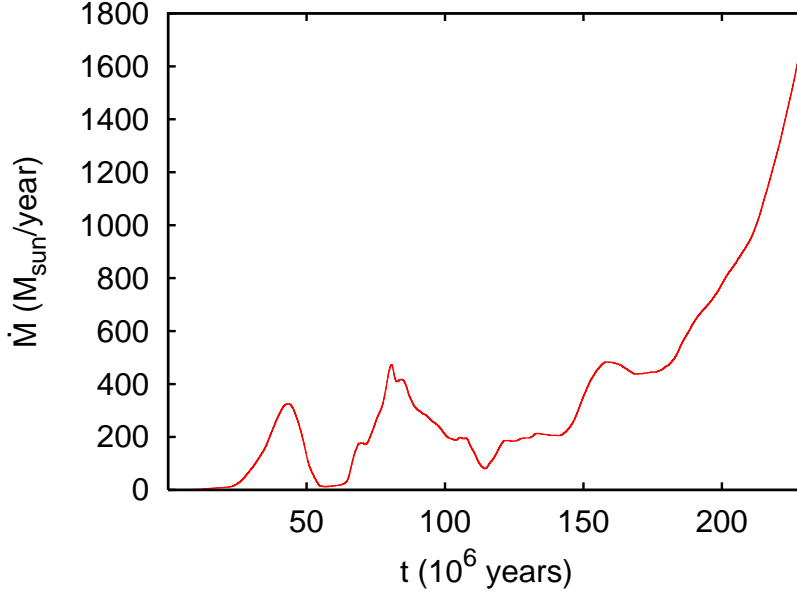


FIG. 7.— Mass accretion rate for low efficiency delayed feedback (Run G).

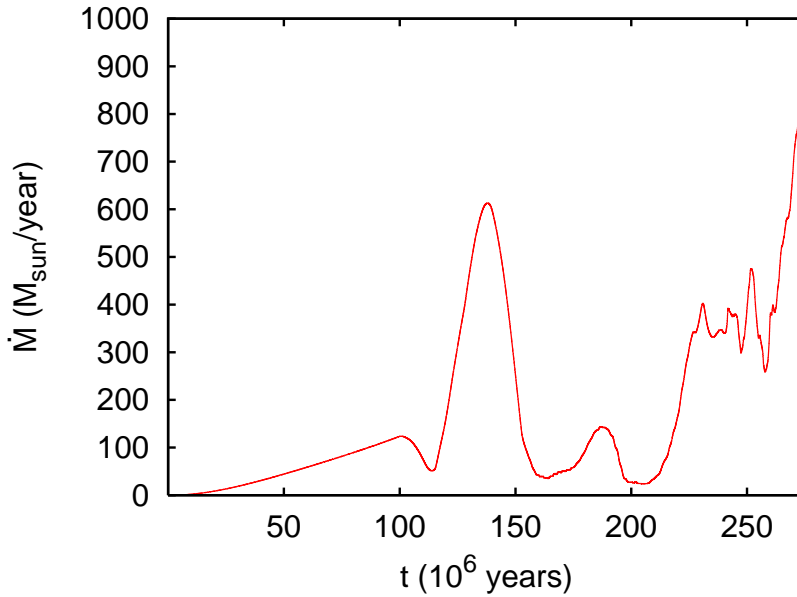


FIG. 8.— Mass accretion rate for low efficiency long delayed feedback (Run I).

well within the ICM core, at which point the angular velocity smoothly goes to zero at the center. Figure 10 from Run M shows the first accretion curve that differs significantly from the previous patterns. Initially, the accretion rate goes up and down in response to the jet. At around 240 Myrs, gas falls below the cooling limit (similar time to the pure cooling and most feedback runs). At 285 Myrs, the accretion passes the  $5000 M_{\odot} \text{year}^{-1}$  limit and continues to climb. Unlike previous setups, it does not grow without bound (or flatten out at some unrealistically high value). Instead at  $16,000 M_{\odot} \text{yr}^{-1}$ , the curve reverses and over the course of 50 Myrs drops back down to very low levels (a few hundreds of solar masses per year. It then continues at that rate with only small

fluctuations for the duration of the simulation.

In this case, the AGN behavior is actually rather incidental. At early times, the slowly rotating inner core of the cluster cools and accretes. Higher angular momentum material flows inwards and, eventually, the ICM core becomes rotationally supported. Given the assumptions of our model, this material will conserve its angular momentum and, irrespective of radiative cooling, will not accrete. The main role of the AGN is to prevent accretion of ICM from the high latitude regions within the centrifugal barrier. Indeed, the cooling catastrophe has *not* in fact been averted. Rapid cooling into a rotationally supported disk can clearly be seen in the late stages of this simulation (Figure 11). Our mass accretion diagnos-

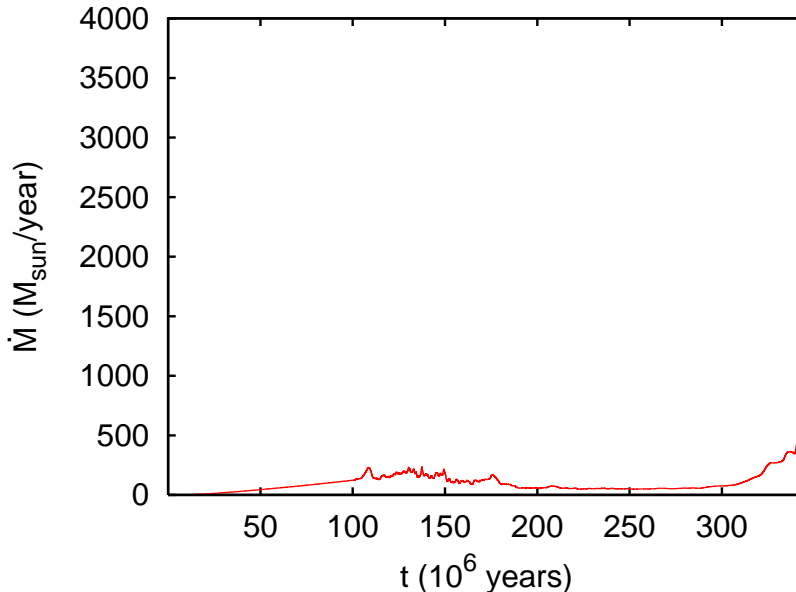


FIG. 9.— Mass accretion rate for very high efficient feedback (Run J).

tic (based on mass flow across the inner radial boundary of the simulation) fails to detect this particular manifestation of the cooling catastrophe.

#### 4. DISCUSSION

Our work with simple hydrodynamic models show that it is more difficult than previously assumed to halt a cooling flow through AGN activity. The ultimate hope (as in the one dimensional models of Ruszkowski & Begelman (2002)) is that through a proper coupling of the AGN to the cluster gas, a long-term balance can be established where the AGN heating balances the ICM radiative cooling. In our three dimensional simulations, we do not see any such balance. Simulations with feedback do not produce many multiple outbursts. Instead they produce one or two long outbursts with varying jet power before the ICM core catastrophically cools.

Our modeled AGN feedback is not totally ineffectual at heating the ICM. Both the time for catastrophic cooling and the time for gas to fall below our cooling limit are increased by the AGN in most cases. The single jet cases are surprisingly effective (delaying the catastrophe for as long the most effective feedback simulations). The instantaneous feedback and the feedback with a delay of the core sound crossing time have basically no effect of the catastrophe time (no more that a few Myrs). The more realistic delays are capable of delaying the cooling catastrophe by several tens of Myrs (more in the unrealistically efficient cases).

There was a single simulations where we appeared to halt catastrophic cooling through the inner simulation boundary. This was the rotating cluster (Run M). As was shown in Figure 10, there is a brief period of very high accretion, following by an extended period of lower accretion. However, as discussed above, catastrophic cooling is still occurring in a rotationally supported disk. The rotational support prevents this gas from falling into the central region, but it is still a large body of cool and cooling gas around the cluster center which contradicts

observations.

Due to the large scale nature of our simulations and the multiple parameters present, it was not possible to test every permutation of the model. It is possible that there is some preferred area of the parameter space where the AGN heating balances the radiative cooling without producing unrealistic jets. The potential existence of such a privileged area of the parameter space does not change our conclusion as it would bring up a serious fine tuning problem. Cooling and AGN occur in a wide range of clusters of varying masses and temperature. For a regulatory mechanism to work, it must be general enough to work in the different clusters. We believe that our simulations sample physically plausible parts of parameter space, thus the failure to model successful AGN feedback is an important result.

Another important consequence of this work is that it firmly underscores the inadequacy of bubble models in any attempt to properly model AGN feedback. Models that involve pre-inflated bubbles, or injecting energy isotropically at given locations in the ICM, will fail to capture precisely that aspect of the physics that turn out to be crucial to the failure of our models — the development of a low density channel along which the AGN outflow can travel unimpeded thereby carrying its kinetic energy out of the cooling core. For this reason, it is vital that the jet dynamics be included if a model is to properly address AGN-halted cooling in a cluster core.

Our results strongly suggest that we must proceed beyond ideal hydrodynamic models if we are to build a successful model of AGN feedback. A very real possibility is that plasma transport processes may be crucial. Thermal conduction provides a way to move thermal energy across a temperature gradient in the ICM and may be essential in helping the system avoid the cooling catastrophe. There is a large heat reservoir in the outer parts of the cluster which could be exploited to warm the core. This would also weaken the requirement that

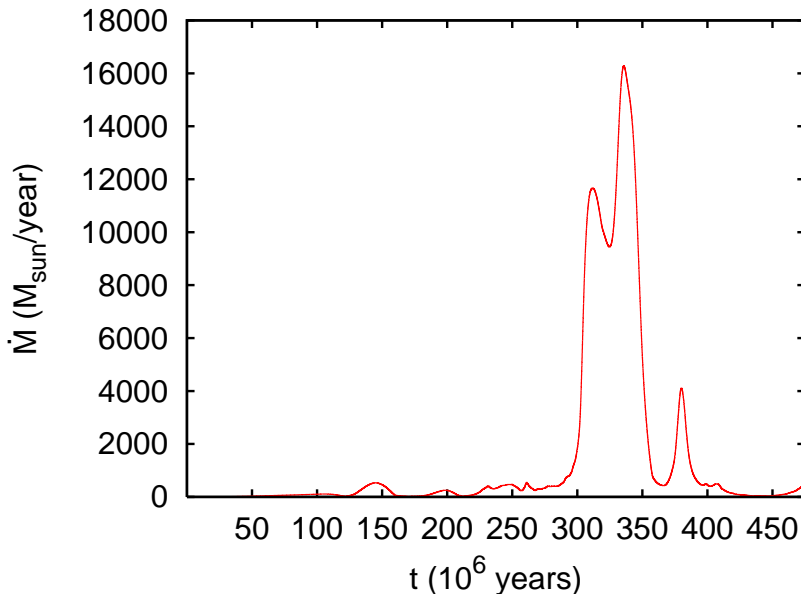


FIG. 10.— Mass accretion rate for rotating cluster with feedback (Run M).

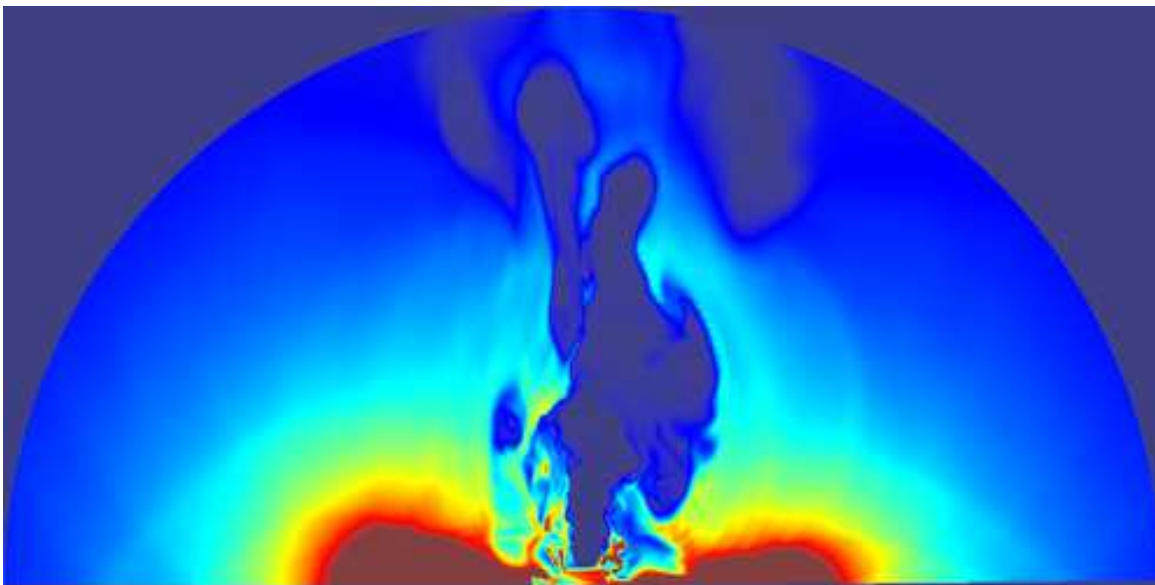


FIG. 11.— Dense cold disk formed in the inner regions of Run M. Density at 880 Myrs shown. Only the inner 254 kpc of the simulation is shown.

AGN deposit energy near the core, possibly enough to halt cooling. There is growing observational evidence for the action of thermal conduction in real clusters (e.g., Perseus-A; Fabian et al. (2005a)).

Magnetic fields are certainly present in the ICM and, at some level, an MHD (or even a kinetic theory) treatment may be necessary. This will have an important effect on the stability of the buoyantly rising bubbles and the mixing of the high entropy radio plasma with the thermal ICM. But magnetic fields may have more profound consequences. Thermal conduction and plasma viscosity will both become very anisotropic due to the suppression of transport processes perpendicular to magnetic field lines, leading to qualitatively new fluid instabilities [the magnetothermal instability (Balbus 2000) and the fire-hose

instability]. In a cooling cluster core with an embedded AGN, one can speculate that these instabilities drive ICM turbulence which may, itself, be a crucial ingredient in the dynamics of the system. Of course, this would be above and beyond any turbulence or bulk motions due to the merging history of the cluster.

Finally, we note that relativistic particles (“cosmic rays”) may play an important role in the thermodynamics of the cluster core (e.g., Chandran (2004)). These particles may originate from the AGN itself or through ICM shocks from AGN activity or merging subclusters.

## 5. CONCLUSION

We have performed a set of high-resolution three dimensional simulations of jetted-AGN embedded in the

cooling ICM cores of galaxy clusters in which the AGN power reacts in response to the cooling of the cluster gas. However, we fail to construct a model in which AGN heating comes into long-term balance with the radiative cooling. The early time jet activity is extremely effective at clearing a channel through the ICM core. The jet at later times flows freely down this channel and hence deposits its kinetic energy well outside the region which is starting to undergo catastrophic cooling. This essential behavior is robust to changing the efficiency or time delay characterizing the AGN feedback. Hence, we argue that physics beyond ideal hydrodynamics is firmly required if any such feedback is to operate successfully. Our results also highlight the absolute necessity to follow the jet dynamics in any attempt to address radio-galaxy

heating of the ICM.

## 6. ACKNOWLEDGMENTS

We thank Sebastian Heinz, Andy Young, and Derek Richardson for extensive discussions throughout the course of this work. We thank the original developers of ZEUS-MP and NCSA for providing the initial code to work with. All simulations reported in this paper were performed on the Beowulf cluster (“The Borg”) supported by the Center for Theory and Computation (CTC) in the Department of Astronomy, University of Maryland, College Park. We gratefully acknowledge support from Cycle-5 Chandra Theory and Modeling Program under grant TM4-5007X.

## APPENDIX

### A. ZEUS-MP

All simulations in this work were done using a modified version of the ZEUS-MP code. Our version is based on the initial NCSA released version (1.0b). Our modifications, documentation, and several supporting scripts have been made publicly available at <http://www.astro.umd.edu/~vernaleo/zeusmp.html> under the same terms as previous ZEUS releases.

Here, we describe our changes and modifications to ZEUS-MP. First, the code had to be ported to compile with a current FORTRAN 77 compiler. As different compilers implement the standard (and the extensions to it) differently, we had to choose certain compilers as our targets. The Intel Compiler was used for the speed of the executables it produces for x86 compatible machines. For the sake of portability, we also maintain compatibility with the GNU compilers. None of these changes modify the behavior of the code. Primarily this involved removing multiply defined variables and cleaning up the namelist routines and the namelists themselves. Also, all filenames that differ only by case (common in the FORTRAN 77 process) were changed to allow building on non-case sensitive filesystems.

To allow for long runs, the restart routines (which did not work for parallel simulations) were completely replaced. The new restart routines work for parallel simulations and write to alternating files to save disk space. A wrapper script written in Perl is provided to correctly pick the most recent restart dump (if present) and start ZEUS-MP using that dump. The wrapper script also performs some basic checks of the integrity of the restart dumps before using them as incomplete or missing restart dumps have proven far more likely in parallel simulations than in single processor simulations.

Despite the fact that ZEUS is written nearly entirely in FORTRAN 77, the C preprocessor is used heavily to allow for conditional inclusion of code. Some portions of this preprocessor code needed to be fixed; many preprocessor directives were not properly matched up or where improperly nested resulting in preprocessor flags that only worked for one of the two possible values. Also, some preprocessor directives did not enclose all of the code relevant to a given option. This made it impossible to completely turn certain options off in the code. The post-processor was modified to be useful for large number of output files and will eventually be completely replaced with a more general post-processor.

Several new problem specific routines were added. A routine to update boundary values during a run was added. A number of other changes and bug-fixes were also made, primarily involving geometry specific bugs. Also, the build process was updated, relying on improved make files and a custom Perl script.

To insure that ZEUS-MP is portable, we have tested and run benchmarks on several different systems. We are aided by the fact that ZEUS uses NCSA’s hdf4 format as its primary output format. By using a portable output format, we do not have to worry about endian issues with our output files. The one place we break this is in the restart dumps which are produced as unformatted FORTRAN binary data. We have run and used ZEUS-MP on a variety of GNU/Linux distributions (both 2.4.x and 2.6.x kernels) on both workstations and a Beowulf cluster. AMD Athlon processors, AMD Opteron processors (in 32 bit mode only as that is all we currently have available), and Intel Pentium 4 processors have primarily been used. We have also compiled and run ZEUS-MP on Apple’s Mac OS X (darwin) on the G4 PowerPC processor. We have also attempted to run ZEUS-MP on a Sun Ultra80 (UltraSPARC II processor) running Solaris 8.0. As we were not able to successfully use the MPI library needed, we were not able to run ZEUS-MP. This is the one weakness in our portability. If a working MPI library (preferably lam-mpi) and the hdf4 library cannot be compiled, ZEUS-MP cannot run on a system. This should not be a problem on any modern, Unix-like system.

#### A.1. Performance

To test performance and scaling, a simulation was run with a  $100^3$  Cartesian grid for 200 time steps in pure hydrodynamics mode with radiative cooling added. This simulation was run as one to eight processes (not necessarily processors). For single processor machines, this means multiple processes on one processor (and presumably a large performance penalty). For the cluster tests this is not a problem. The timing results are shown in Figure A12. There are two surprises in these results. The first is that at 8 processors, code compiled with the GNU compilers seems to

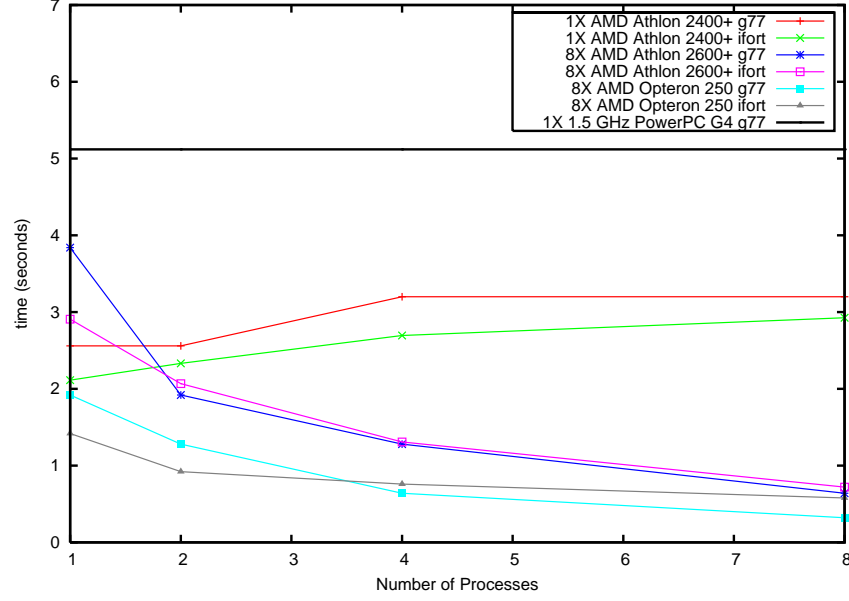


FIG. A12.— ZEUS-MP run time benchmarks for a variety of processors on a  $100^3$  cell grid.

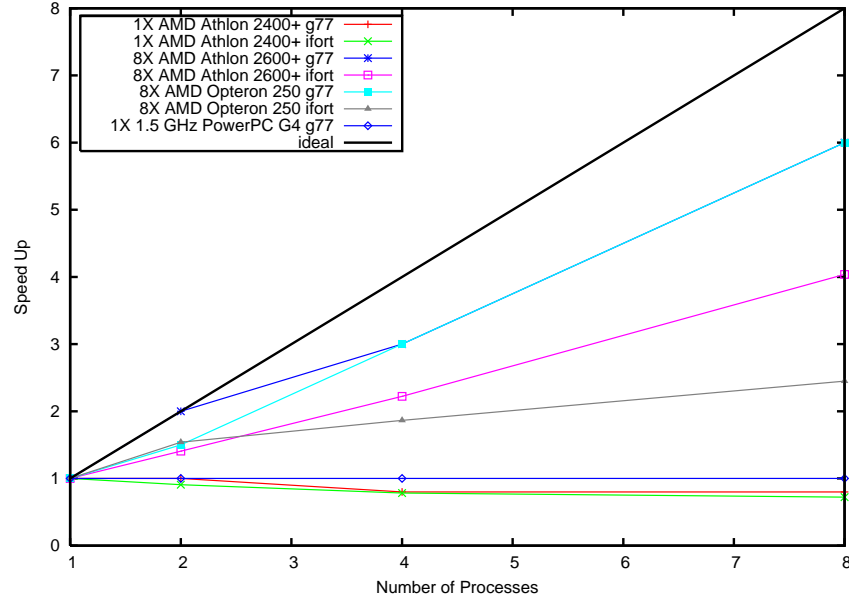


FIG. A13.— ZEUS-MP speed up tests for a variety of processors on a  $100^3$  cell grid along with the theoretical performance.

outperform the code from the Intel compiler (when used on AMD processors). This is surprising as the Intel compiler is widely considered to produce the fastest code for x86 processors. The second surprising feature is that the G4, while it performs far below anything else in the tests, does not appear to have any penalty for multiple processes on a single processor.

The results from the scaling test are shown in Figure A13. While at no point beyond two processors do we get the theoretical linear increase, we continue to get a decent speedup (with a constant slope in most cases) up to at least 8 processors, with the code produced with the GNU compiler getting much closer to linear than the Intel compiler.

#### REFERENCES

- Armitage, P. J. & Reynolds, C. S. 2003, MNRAS, 341, 1041  
 Bîrzan, L., Rafferty, D. A., McNamara, B. R., Wise, M. W., & Nulsen, P. E. J. 2004, ApJ, 607, 800  
 Balbus, S. A. 2000, ApJ, 534, 420  
 Basson, J. F. & Alexander, P. 2003, MNRAS, 339, 353  
 Benson, A. J., Bower, R. G., Frenk, C. S., Lacey, C. G., Baugh, C. M., & Cole, S. 2003, ApJ, 599, 38  
 Blanton, E. L., Sarazin, C. L., McNamara, B. R., & Wise, M. W. 2001, ApJ, 558, L15

- Böhringer, H., Nulsen, P. E. J., Braun, R., & Fabian, A. C. 1995, *MNRAS*, 274, L67
- Böhringer, H., Voges, W., Fabian, A. C., Edge, A. C., & Neumann, D. M. 1993, *MNRAS*, 264, L25
- Brüggen, M. & Kaiser, C. R. 2001, *MNRAS*, 325, 676
- . 2002, *Nature*, 418, 301
- Burns, J. O. & Owen, F. N. 1977, *ApJ*, 217, 34
- Carilli, C. L., Perley, R. A., & Harris, D. E. 1994, *MNRAS*, 270, 173
- Chandran, B. D. G. 2004, *ApJ*, 616, 169
- Choi, Y., Reynolds, C. S., Heinz, S., Rosenberg, J. L., Perlman, E. S., & Yang, J. 2004, *ApJ*, 606, 185
- Churazov, E., Brüggen, M., Kaiser, C. R., Böhringer, H., & Forman, W. 2001, *ApJ*, 554, 261
- Clarke, D. A., Harris, D. E., & Carilli, C. L. 1997, *MNRAS*, 284, 981
- Dekel, A. & Silk, J. 1986, *ApJ*, 303, 39
- Fabian, A. C. 1994, *ARA&A*, 32, 277
- Fabian, A. C., Reynolds, C. S., Taylor, G. B., & Dunn, R. J. H. 2005a, *MNRAS*, 363, 891
- Fabian, A. C., Sanders, J. S., Allen, S. W., Crawford, C. S., Iwasawa, K., Johnstone, R. M., Schmidt, R. W., & Taylor, G. B. 2003, *MNRAS*, 344, L43
- Fabian, A. C., Sanders, J. S., Ettori, S., Taylor, G. B., Allen, S. W., Crawford, C. S., Iwasawa, K., Johnstone, R. M., & Ogle, P. M. 2000, *MNRAS*, 318, L65
- Fabian, A. C., Sanders, J. S., Taylor, G. B., & Allen, S. W. 2005b, *MNRAS*, 360, L20
- Feigelson, E. D., Wood, P. A. D., Schreier, E. J., Harris, D. E., & Reid, M. J. 1987, *ApJ*, 312, 101
- Felten, J. E., Gould, R. J., Stein, W. A., & Woolf, N. J. 1966, *ApJ*, 146, 955
- Gammie, C. F. 1999, *ApJ*, 522, L57
- Heinz, S., Choi, Y., Reynolds, C. S., & Begelman, M. C. 2002, *ApJ*, 569, L79
- Heinz, S., Reynolds, C. S., & Begelman, M. C. 1998, *ApJ*, 501, 126
- Jones, T. W. & De Young, D. S. 2005, *ApJ*, 624, 586
- Larson, R. B. 1974, *MNRAS*, 169, 229
- McNamara, B. R., Wise, M., Nulsen, P. E. J., David, L. P., Sarazin, C. L., Bautz, M., Markevitch, M., Vikhlinin, A., Forman, W. R., Jones, C., & Harris, D. E. 2000, *ApJ*, 534, L135
- McNamara, B. R., Wise, M. W., Nulsen, P. E. J., David, L. P., Carilli, C. L., Sarazin, C. L., O’Dea, C. P., Houck, J., Donahue, M., Baum, S., Voit, M., O’Connell, R. W., & Koekemoer, A. 2001, *ApJ*, 562, L149
- Novikov, I. D. & Thorne, K. S. 1973, in *Black Holes*, ed. C. DeWitt & B. DeWitt (Gordon and Breach, Paris), 343–450
- O’Dea, C. P., Baum, S. A., Mack, J., Koekemoer, A. M., & Laor, A. 2004, *ApJ*, 612, 131
- Ostriker, J. P., Bode, P., & Babul, A. 2005, *ArXiv Astrophysics e-prints*
- Rees, M. J. & Ostriker, J. P. 1977, *MNRAS*, 179, 541
- Reynolds, C. S., Heinz, S., & Begelman, M. C. 2002, *MNRAS*, 332, 271
- Reynolds, C. S., McKernan, B., Fabian, A. C., Stone, J. M., & Vignale, J. C. 2005, *MNRAS*, 357, 242
- Robinson, K., Dursi, L. J., Ricker, P. M., Rosner, R., Calder, A. C., Zingale, M., Truran, J. W., Linde, T., Caceres, A., Fryxell, B., Olson, K., Riley, K., Siegel, A., & Vladimirova, N. 2004, *ApJ*, 601, 621
- Ruszkowski, M. & Begelman, M. C. 2002, *ApJ*, 581, 223
- Ruszkowski, M., Brüggen, M., & Begelman, M. C. 2004, *ApJ*, 615, 675
- Stone, J. M. & Norman, M. L. 1992a, *ApJS*, 80, 753
- . 1992b, *ApJS*, 80, 791
- Sutherland, R. S. & Dopita, M. A. 1993, *ApJS*, 88, 253
- Young, A. J., Wilson, A. S., & Mundell, C. G. 2002, *ApJ*, 579, 560